**ECTI Transactions on Computer and Information Technology**
Journal homepage: https://ph01.tci-thaijo.org/index.php/ecticit/
Published by the ECTI Association, Thailand, ISSN: 2286-9131

# Horn and Schunck Optical Flow Robustness on Non-Gaussian Noise by Fine-Tune Lorentzian Norm Influence Function

Darun Kesrarat[1], Vorapoj Patanavijit[2] and Kornkamol Thakulsukanant[3]

## ABSTRACT

The noise sensitivity of the optical flow is a limitation for determining the motion flow. When there is noise, the optical flow cannot identify the outcome of the motion flow. The robustness strategy using the fine-tuned Lorentzian function is provided here to strengthen the resilience of the optical flow's effect. In dense processing, when non-Gaussian disturbances are present in opposition to each frame of the input video sequence, we concentrate on the realization of the Horn and Schunck optical flow technique. The error in the motion flow is evaluated by calculating the Error Vector Magnitude (EVM) value. The EVM considers the motion flow's faultlessness in both range and direction. We simulated several non-Gaussian noises over a range of input video sequences for the evaluation. By employing the fine-tuning Lorentzian norm influence function on the Horn and Schunk optical flow, we could determine how the robustness of the motion flow had improved.

*Article information:*

**Keywords:** Horn and Schunck Optical Flow, Lorentzian Norm Influence Function, Non-Gaussian Noise, Error Vector Magnitude

**Article history:**
Received: September 12, 2023
Revised: November 23, 2023
Accepted: December 7, 2023
Published: December 23, 2023 (Online)

**DOI:** 10.37936/ecti-cit.2023174.254112

## 1. INTRODUCTION

The method for detecting motion in video sequences is called optical flow [1, 2]. In the past three decades, many approaches have been presented for figuring motion vectors, including the Block-based technique [3], the Lucas and Kanade technique [4], and the Phased-correlation technique [5]. However, the Horn and Schunck technique (H-S) [6] is one of the optical flow techniques for figuring out the motion vector of every pixel in a sequence of images. While many techniques have been proposed to solve this problem, H-S stands out as one of the most efficient ones for real-time processing, and it was used by many areas of research and applications such as Real-Time Efficient FPGA for 4K Video Stream [7] and Motion Estimating Optical Flow for Action Recognition [8]. In the H-S technique, the global idea, where the missing motion detail in inner sections from the motion frames of the solid objects is filled in, yields a high density of motion flow. However, the biggest flaw is an increased high noise sensitivity.

The output of the motion flow from optical flow was employed as an input in many fields of advanced study and application, including picture compression [9, 10], motion tracking [11], object detection [12], video encoding [13, 14], consistent estimation in real environment [15], and image super-resolution [16]. Then, quality in the accuracy of the optical flow directly affects the performance of these applications in consequence.

In most areas of image and video processing, noise was the problem. When noise is present over picture and video sources, the overall performance is affected depending on numerous variables, including the type and quantity of noise. When noise interferes with video sequences in optical flow, the range and direction of the motion flow are faulty. As said, the optical flow's primary flaw is its sensitivity to noise. There are two basic options to lessen these issues. The first is the pre-processing technique. It involves using a typical image noise reduction model to reduce noise from the input video sequence [17–19] before submitting it for processing in an optical flow. However, this approach takes longer to complete because noise removal processing and noise type/level detection are required. Additionally, the noise removal technique

[1] The author is with Vincent Mary School of Science and Technology, Assumption University, Thailand, Email: darunksr@gmail.com
[2] The author is with Faculty of Engineering, Assumption University, Thailand, Email: Patanavijit@yahoo.com
[3] The author is with Martin de Tours School of Management and Economics, Assumption University, Thailand, Email: kthakulsukanant@yahoo.com

can occasionally lose the image's primary content. The second is a post-processing technique by the reliable method that processes bilateral function and median function in addition to optical flow in computing [20]. However, they still showed a significant lack of consistency when determining motion flow.

This work concentrates on the H-S technique in dense processes to address the robust post-processing technique. We modify the Lorentzian norm function [21] into a fine-tuned Lorentzian norm influence function in conjunction with the H-S to improve the optical flow's robustness in determining the range and direction of the motion flow over a variety of non-Gaussian noise types, including Poisson, Salt-Pepper, and Speckle. We also analyze how each robust technique is affected by the differentiating features of the video sequence. In our experiment, we compared the level of robustness with other post-processing robustness methods while opposing the non-Gaussian noise over various characteristic standard video sequences. We also studied the robustness level from multiple characteristics of video sequences on each type of non-Gaussian noise by determining the fault in the range and direction of the motion flow through the EVM.

The order of the paper is as follows. The literature overview for optical flow techniques and post-processing robustness techniques is presented in Part 2. The robustness level experiment result from the Error Vector Magnitude EVM is shown in Part 3. The conclusion is presented in Part 4.

## 2. TECHNIQUES FOR OPTICAL FLOW AND POST-PROCESSING ROBUSTNESS

This section describes the resilience methods in optical flow and the Horn and Schunck optical flow technique.

### 2.1 The H-S Technique

A traditional optical flow method that is used to compute motion between two frames is the H-S [8]. H-S calculates the smoothness flow across the entire image. It reduces flow distortions. For sequences of two-dimensional image files, this function is defined. For each pixel in the image, the linear motion flow ($\mathbf{u}$ and $\mathbf{v}$) is calculated using:

$$\boldsymbol{u}^{k+1} = \bar{\boldsymbol{u}}^{k} - \frac{I_x[I_x\bar{\boldsymbol{u}}^{k} + I_y\bar{\boldsymbol{v}}^{k} + I_t]}{\alpha^2 + I_x^2 + I_y^2} \tag{1.1}$$

$$\boldsymbol{u}^{v+1} = \bar{\boldsymbol{v}}^{k} - \frac{I_y[I_x\bar{\boldsymbol{u}}^{k} + I_y\bar{\boldsymbol{v}}^{k} + I_t]}{\alpha^2 + I_x^2 + I_y^2} \tag{1.2}$$

Where the corresponding values, initially set to 0, must be repeated $k$ times to reduce the total of mistakes, an iterative calculation is required to optimize the process with the suitable smoothness weight $(\alpha)$.$\bar{\boldsymbol{u}}^{k}$ and $\bar{\boldsymbol{v}}^{k}$ are the average vector at time $k$. In Fig. 1, image sequence number t is represented by the gradient intensity (brightness) $I(x, y, t)$.

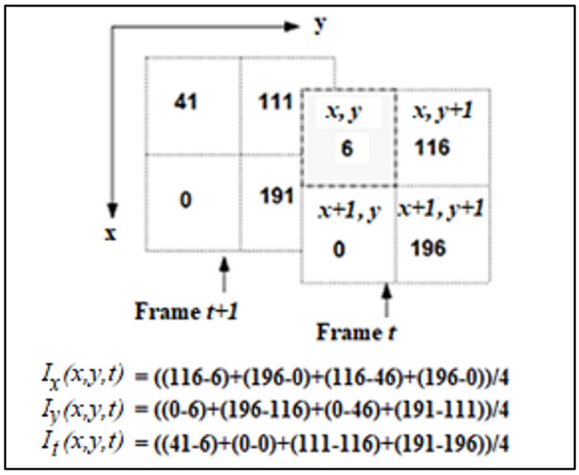


***Fig.1:*** *The calculation of brightness constancy.*

The spatiotemporal image gradient is used to resolve the brightness constancy $(I_x, I_y, I_t)$ using:

$$\begin{aligned} I_x =& 1/4\{I(x,y+1,t) - I(x,y,t) + I(x+1,y+1,t) - I(x+1,y,t) \\ &+ I(x,y+1,t+1) - I(x,y,t+1) + I(x+1,y+1,t+1) \\ &- I(x+1,y,t+1)\} \end{aligned} \tag{2.1}$$

$$\begin{aligned} I_y =& 1/4\{I(x+1,y,t) - I(x,y,t) + I(x+1,y+1,t) - I(x,y+1,t) \\ &+ I(x+1,y,t+1) - I(x,y,t+1) + I(x+1,y+1,t+1) \\ &- I(x,y+1,t+1)\} \end{aligned} \tag{2.2}$$

$$\begin{aligned} I_t =& 1/4\{I(x,y,t+1) - I(x,y,t) + I(x+1,y,t+1) - I(x+1,y,t) \\ &+ I(x,y+1,t+1) - I(x,y+1,t) + I(x+1,y+1,t+1) \\ &- I(x+1,y+1,t)\} \end{aligned} \tag{2.3}$$

Where $x$ and $y$ are the coordinate positions of the focus pixel and $t$ is the no. of the image sequence.

The H-S provides quick and reliable results in the estimated MV due to the performance inspection [21]. However, it is pretty noise-sensitive. When noises are present in the input video sequence, the H-S algorithm produces a fairly flat result, and each video sequence characteristic should be considered when using the smoothness weight $(\alpha)$.

### 2.2 Gradient orientation of L1 median on H-S (M-HS)

This post-processing method makes the optical flow more resilient by adding the L1 median filter to the input image sequence, which protects it from noise. In general, the L1 median function is used in parts of standard image processing to deal with general noise. To increase the robustness of optical flow, this normalization form has used post-processing with the results of the H-S's motion flow [20].

$$(\boldsymbol{u}_{L1}, (v)_{L1}) = \left(\frac{\boldsymbol{u}}{|\boldsymbol{u}|}, \frac{\boldsymbol{v}}{|\boldsymbol{v}|}\right) \tag{3}$$

When two scalar limits between -1 and 1 are placed on the motion flow $\boldsymbol{u}_{L1}$ and $\boldsymbol{v}_{L1}$, motion flow is constrained. In the application field where we anticipate the direction but not the range, it is appropriate to use the result of M-HS with constrained scalar. Additionally, it functions effectively on the input video sequence with moderate movement.

### 2.3 Bilateral Filter on H-S (B-HS)

This filter performed post-processing to the H-S motion flow result [26] to increase optical flow resilience. In this method, a bilateral filter [22] is a smoothing filter used in several fields of image processing, including noise reduction [23–25]. The definition of the bilateral filter on H-S is:

$$v_b = \frac{1}{k}\sum_{|m|<M} v\varnothing(x+m) \tag{4}$$

$$K = \sum_{|m|<M} \varnothing(x+m) \tag{5}$$

$$\varnothing(x+n) = \exp\left(\frac{|n|^2}{2\delta_a^2} + \frac{|I(x+n)-I(x)^2|}{2\delta_b^2}\right) \tag{6}$$

Where $\boldsymbol{v}_b$ is the motion vector of B-HS. M is the neighbour flow interval (in our experiment, we fixed M to be 7). The motion flow of H-S is $\boldsymbol{v}$. The bilateral filter normalized kernel is $K$. The Gaussian kernel is $\varnothing$. And $\delta_b$ is the brightness standard deviation of $I(x)$ (in our experiment, we set the deviation in $\delta_a$ as $\boldsymbol{v} \times 7$) with the iterative bilateral filter's smoothness weight characteristic. When we used the H-S, it kept the robustness as well.

### 2.4 Fine-Tune Lorentzian Norm Influence Function on H-S (L-HS)

One of the reliable error functions [27, 28] to reject and stop the outliers created by system disturbances is the Lorentzian. By decreasing the error in super image reconstruction, the Lorentzian function was employed in the past to enhance estimation [29]. This function applied post-processing optical flow [21] to increase optical flow resilience in L-HS. Regarding the value of parameter $T$, most of the clear and interfered sequences in our experiment show the best average in performance where $T$ is equal to 1.25. When we use the Fine-Tune Lorentzian Norm Influence with the H-S (we set $T$ as 1.25 in our experiment), it exhibits greater resilience, as seen in Fig. 2.

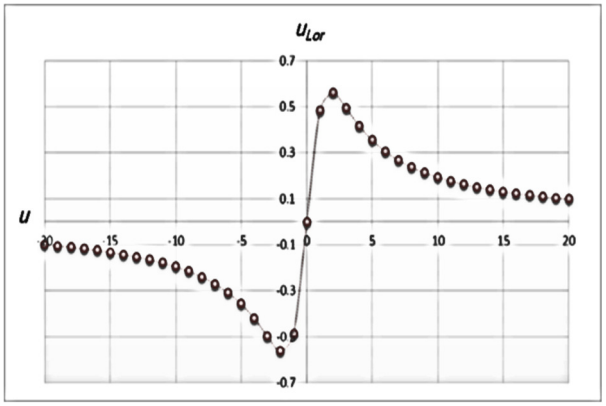


***Fig.2:*** *The fine-tune influence function of The Lorentzian norm (T=1.25).*

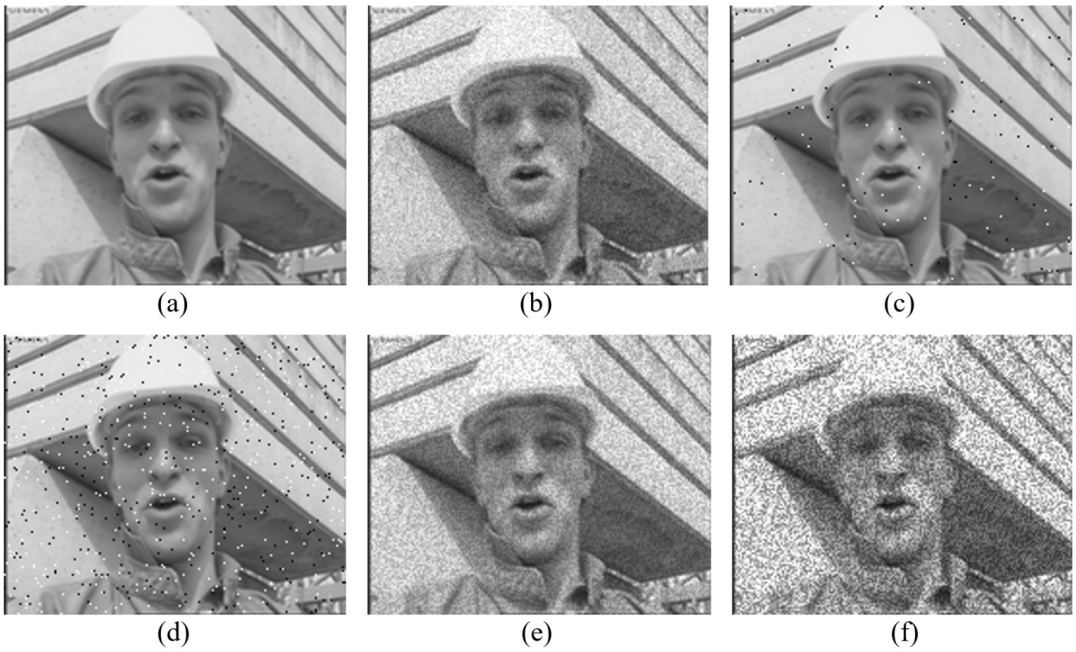


***Fig.3:*** *Combined image with non-Gaussian noises (a) non-noise, (b) Poisson, (c) Salt-Pepper (density 0.005), (d) Salt-Pepper (density 0.005), (e) Speckle (variance 0.01), and (f) Speckle (variance 0.05).*

Equation (7) defines the Lorentzian norm. Then, for increased robustness, the Lorentzian norm was transformed into the Lorentzian norm influence function and processed alongside the optical flow. Equation (8) defines the Lorentzian norm effect function.

$$\mathbf{P}_{Lor} = \log\left[1 + \frac{1}{2}\left(\frac{\mathrm{u}}{T}\right)^2\right] \tag{7}$$

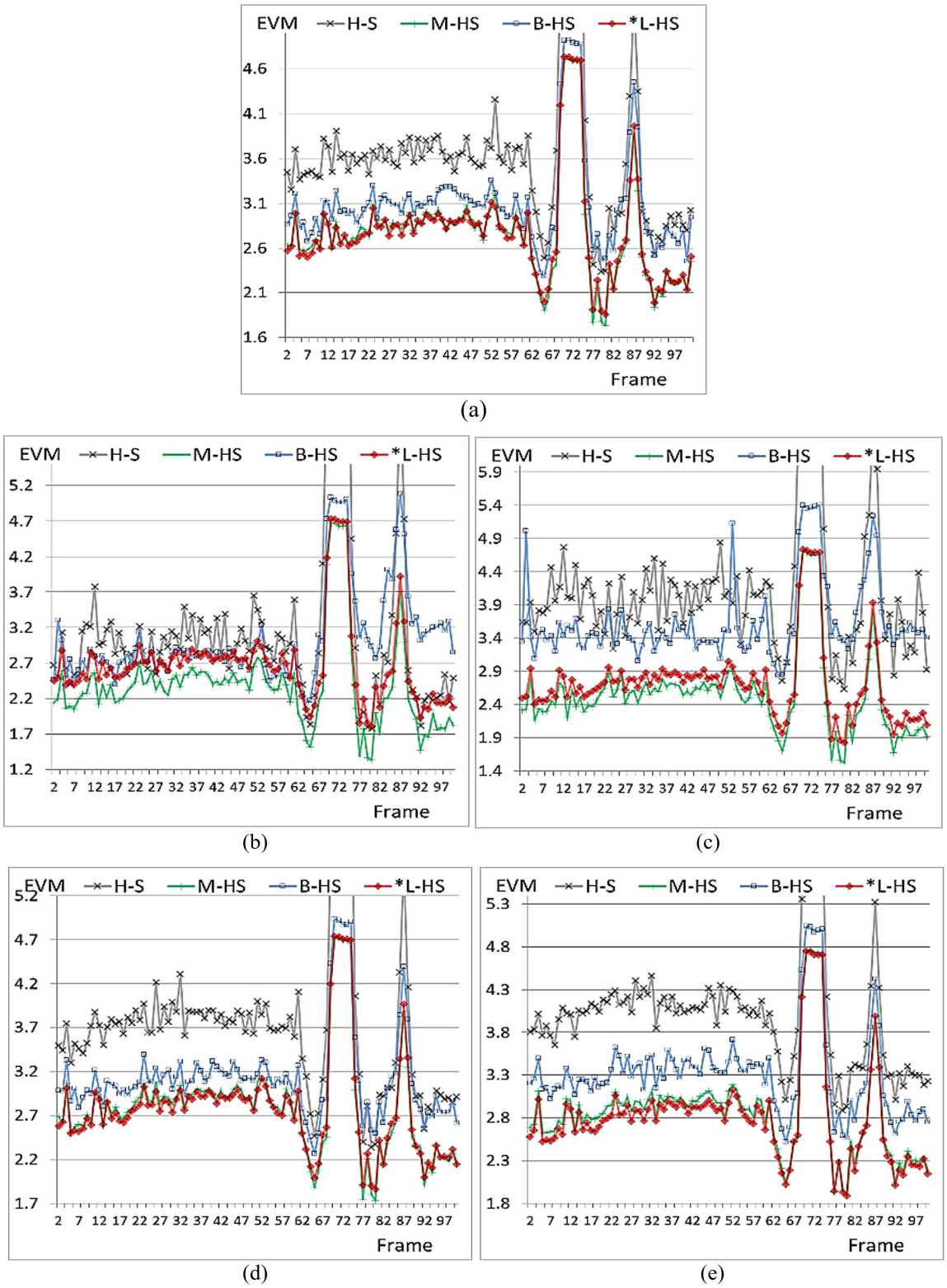


***Fig.4:*** *Each COASTGUARD image frame's EVM results for (a) Poisson, (b) Salt-Pepper (density 0.005), (c) Salt-Pepper (density 0.025), (d) Speckle (variance 0.01), and (e) Speckle (variance 0.05) are shown.*

$$\mathbf{u}_{Lor} = \left( \frac{2 \times \mathrm{u}}{(2 \times T^2) + \mathrm{u}^2} \right) \tag{8}$$

Where $T$ is the scale factor that we run this parameter using several values in our experiment.

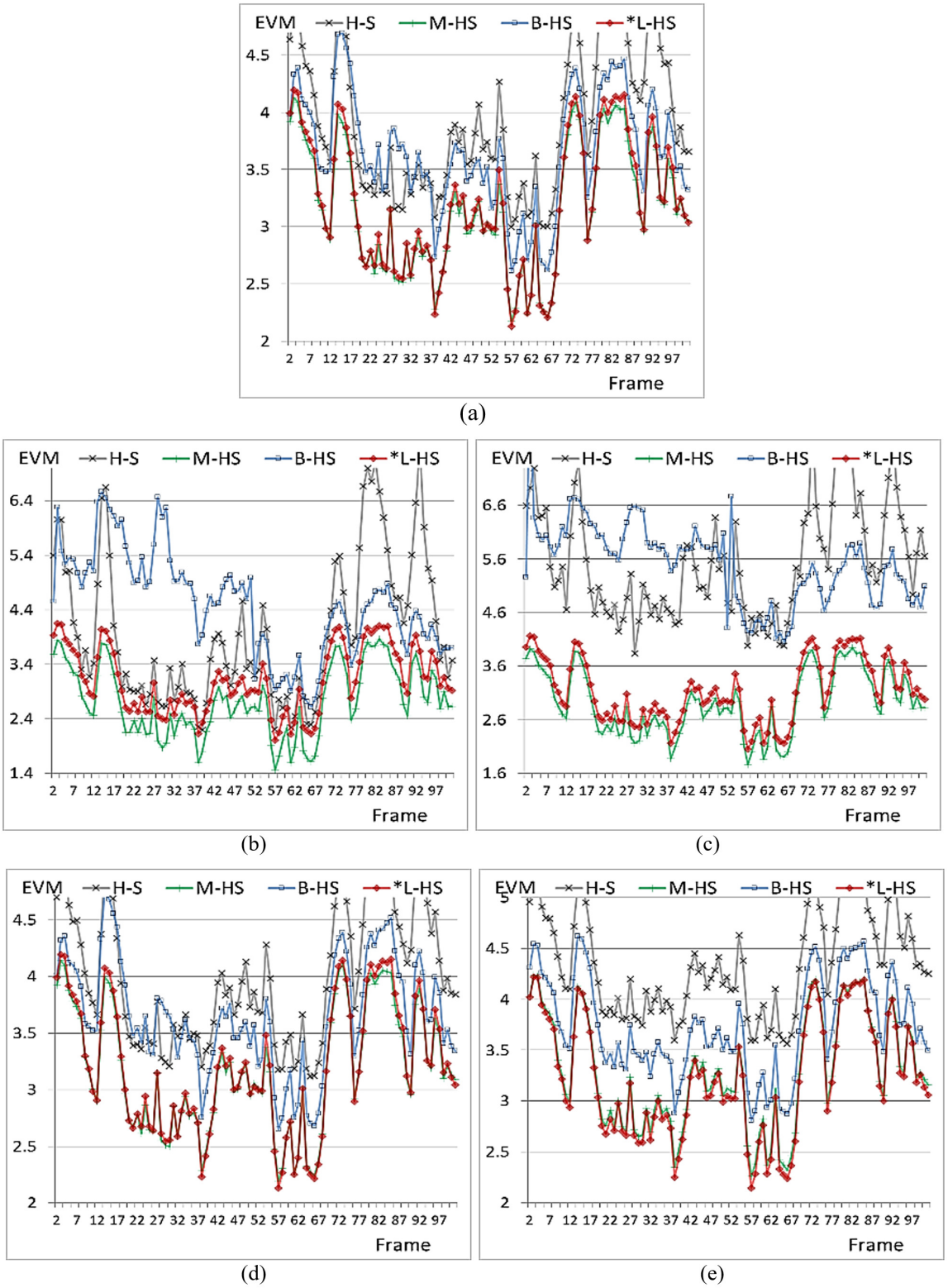


***Fig.5:*** *Each FOREMAN image frame's EVM results for (a) Poisson, (b) Salt-Pepper (density 0.005), (c) Salt-Pepper (density 0.025), (d) Speckle (variance 0.01), and (e) Speckle (variance 0.05) are shown.*

## 3. RESULTS OF THE EXPERIMENT

For our investigation, we generated four standard sets of input video sequences (each video can contain up to 100 image frames). Two video clips with rapid movement, like COASTGUARD and FOREMAN. And two video clips with slow motion, such as AKIYO and CONTAINER. Poisson, Salt-Pepper (density 0.005), Salt-Pepper (density 0.025), Speckle

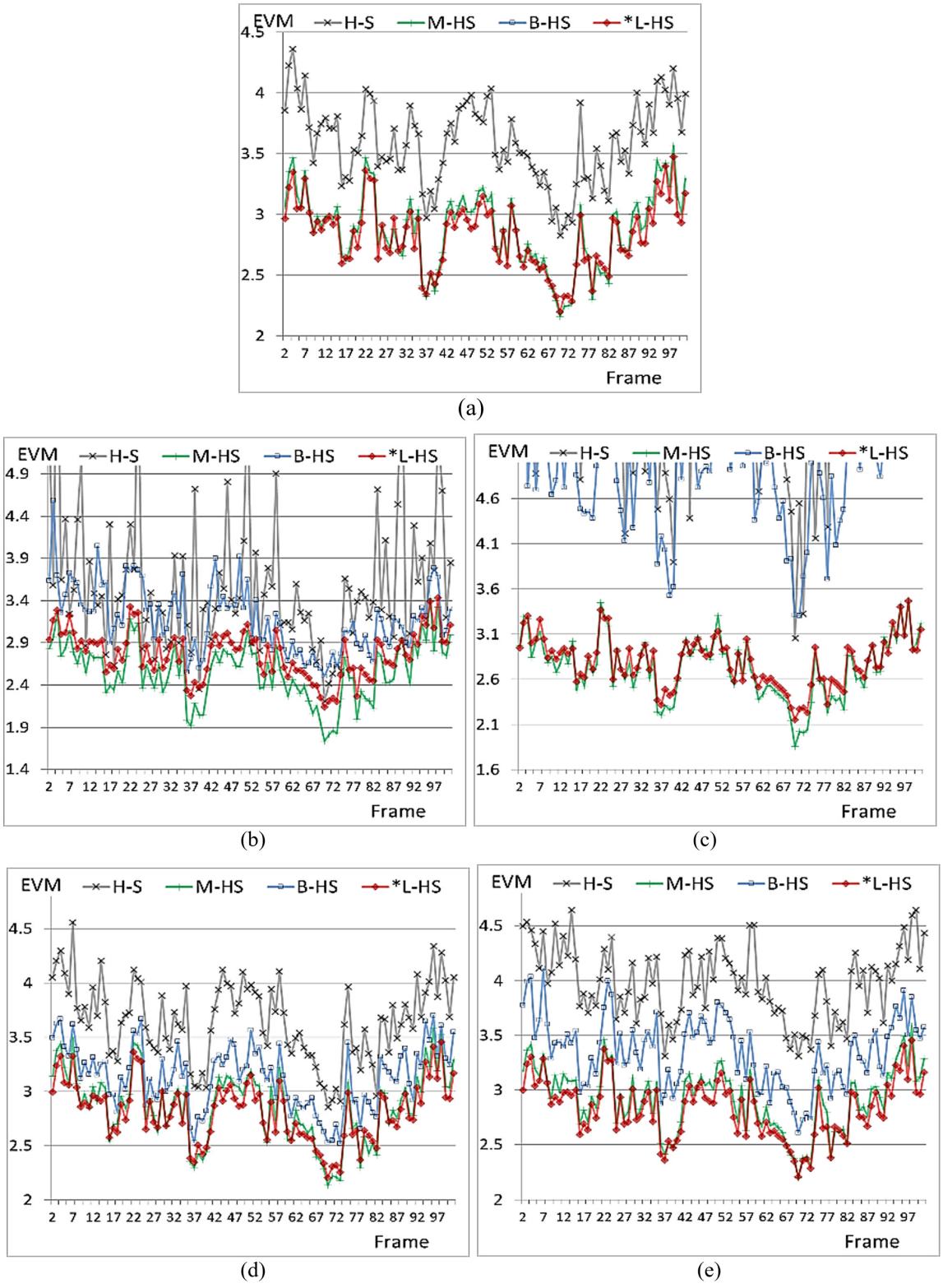


***Fig.6:*** *Each AKIYO image frame's EVM results for (a) Poisson, (b) Salt-Pepper (density 0.005), (c) Salt-Pepper (density 0.025), (d) Speckle (variance 0.01), and (e) Speckle (variance 0.05) are shown.*

noise (variance 0.01), and Speckle noise (variance 0.05) are the five non-Gaussian noise types that were combined into the video sequences. Fig.3(a) illustrates the non-noise. Fig.3(b) illustrates the Poisson noise. Fig.3(c) shows the Salt-Pepper noise at density 0.005. Fig.3(d) shows the Salt-Pepper noise at density 0.025. Fig.3(e) shows the Speckle noise at variance 0.01. And Fig.3(f) shows the Speckle noise at variance 0.05.

To estimate brightness for H-S, we fixed the

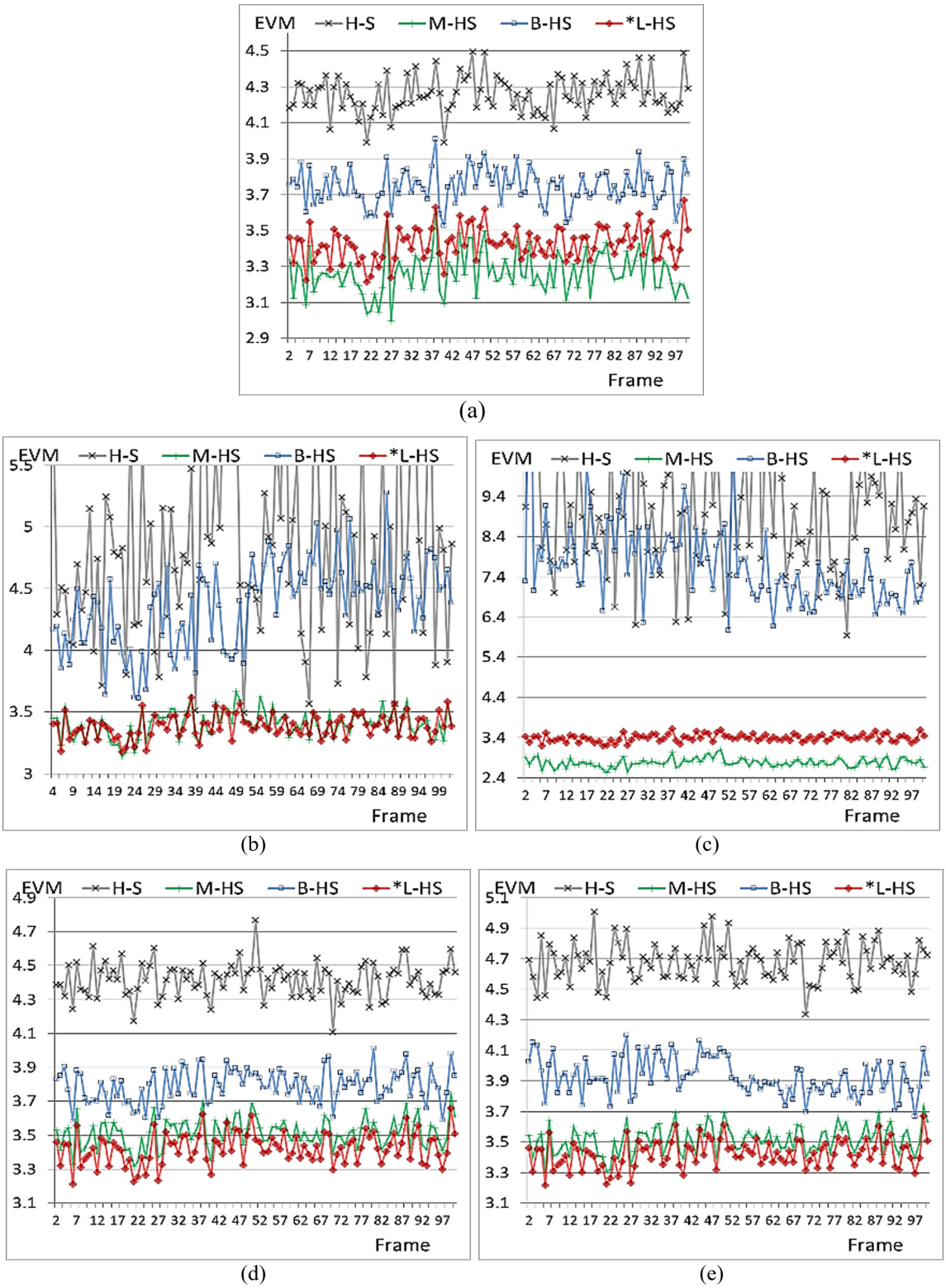


***Fig.7:*** *Each CONTAINER image frame's EVM results for (a) Poisson, (b) Salt-Pepper (density 0.005), (c) Salt-Pepper (density 0.025), (d) Speckle (variance 0.01), and (e) Speckle (variance 0.05) are shown.*

smoothness weight at 0.5 and used the BFB mask coefficient [30] at 100 iterations, which is identical to the specification in the function of BFB. As a result of our experiment, we calculated the Error Vector Magnitude (EVM) value by considering only the active movement vector from the ground truth vector in the evaluation. We adopted the EVM because its ability to reflect meaning in the range and direction of motion flow-where a lower rate EVM indicates stronger robustness-led to its employment. In our experiment, we compare the result MV with the origin MV and use root-mean-square to calculate the average inaccuracy from the movement vector.

We declared the EVM results for each image frame from the input video sequence in Figs. 4 through 7 to specifically highlight the robustness level. We experimented with the COASTGUARD sequence in Fig. 4. Fig.4(a) illustrates the Poisson finding. In Fig.4(b) and Fig.4(c), the outcome for Salt-Pepper (density 0.005 and 0.025) is shown. In Fig.4(d) and Fig.4(e),

***Table 1:*** *The EVM's mean and standard deviation.*

| Noise Type | Method | COASTGUARD | | FOREMAN | | AKIYO | | CONTAINER | |
|---|---|---|---|---|---|---|---|---|---|
| | | AVG EVM | SD of EVM | AVG EVM | SD of EVM | AVG EVM | SD of EVM | AVG EVM | SD of EVM |
| Poisson | H-S | 3.636 | 0.959 | 3.924 | 0.642 | 3.585 | 0.334 | 4.257 | 0.103 |
| | M-HS | **2.777** | 0.590 | **3.159** | 0.550 | 2.868 | 0.316 | **3.266** | 0.116 |
| | B-HS | 3.105 | **0.539** | 3.653 | **0.507** | 3.138 | 0.304 | 3.746 | 0.099 |
| | ***L-HS** | 2.786 | 0.584 | 3.201 | 0.579 | **2.818** | **0.275** | 3.426 | **0.092** |
| Salt-Pepper (density 0.005) | H-S | 3.269 | 1.624 | 3.986 | 1.331 | 3.591 | 0.870 | 4.861 | 0.820 |
| | M-HS | **2.402** | 0.664 | **2.744** | 0.647 | **2.563** | 0.348 | 3.398 | 0.111 |
| | B-HS | 3.054 | 0.670 | 4.518 | 0.950 | 3.188 | 0.399 | 4.386 | 0.357 |
| | ***L-HS** | 2.696 | **0.593** | 3.115 | **0.599** | 2.769 | **0.284** | **3.384** | **0.094** |
| Salt-Pepper (density 0.025) | H-S | 4.211 | 1.356 | 5.542 | 1.052 | 6.407 | 1.635 | 9.063 | 1.556 |
| | M-HS | **2.556** | 0.632 | **2.926** | 0.599 | **2.725** | 0.335 | **2.778** | 0.111 |
| | B-HS | 3.653 | 0.601 | 5.526 | 0.779 | 5.215 | 1.164 | 7.736 | 1.203 |
| | ***L-HS** | 2.732 | **0.590** | 3.154 | **0.591** | 2.788 | **0.279** | 3.395 | **0.094** |
| Speckle (variance 0.01) | H-S | 3.731 | 0.965 | 4.010 | 0.607 | 3.647 | 0.364 | 4.415 | 0.103 |
| | M-HS | 2.797 | 0.592 | **3.178** | 0.551 | 2.861 | 0.330 | 3.514 | **0.088** |
| | B-HS | 3.136 | **0.521** | 3.669 | **0.503** | 3.133 | 0.293 | 3.795 | 0.098 |
| | ***L-HS** | **2.791** | 0.583 | 3.206 | 0.578 | **2.814** | **0.277** | **3.423** | 0.092 |
| Speckle (variance 0.05) | H-S | 4.012 | 0.720 | 4.355 | 0.502 | 3.980 | 0.333 | 4.679 | 0.128 |
| | M-HS | 2.874 | 0.573 | 3.284 | 0.558 | 2.911 | 0.294 | 3.516 | 0.092 |
| | B-HS | 3.321 | **0.519** | 3.743 | **0.487** | 3.353 | 0.320 | 3.928 | 0.121 |
| | ***L-HS** | **2.809** | 0.580 | **3.234** | 0.579 | **2.829** | **0.268** | **3.424** | **0.092** |

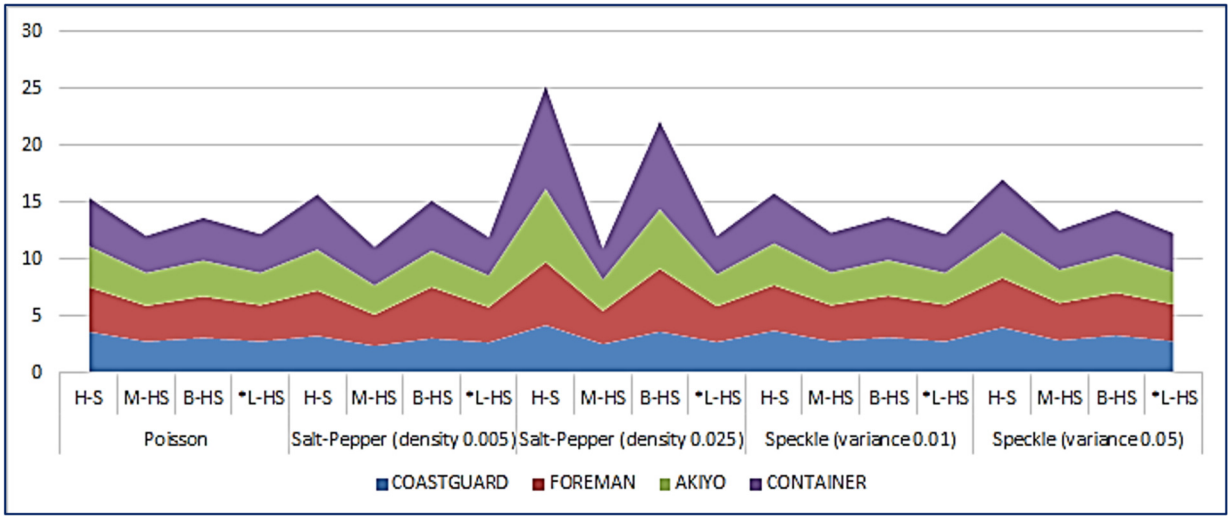


***Fig.8:*** *The analyzed graph represented the level of average EVM from each technique against each type of non-Gaussian noise for each video sequence.*

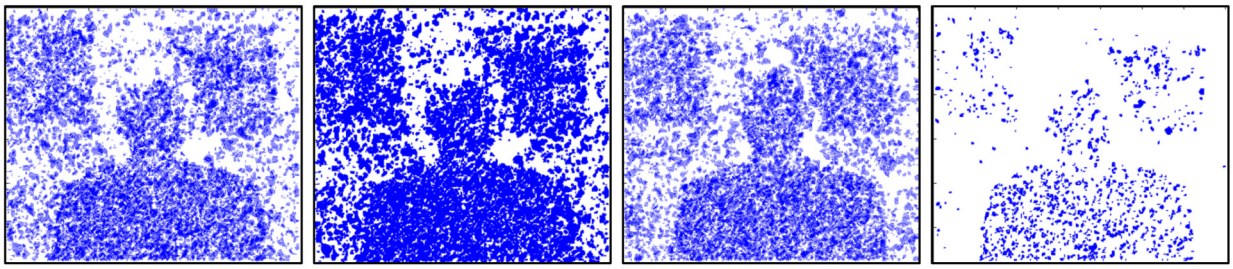


***Fig.9:*** *The optical flow vectors of the AKIYO image frame no. 50 which it is interfered by Speckle noise (variance 0.05) processed by (a) H-S, (b) M-HS, (c) B-HS, and (d) L-HS.*

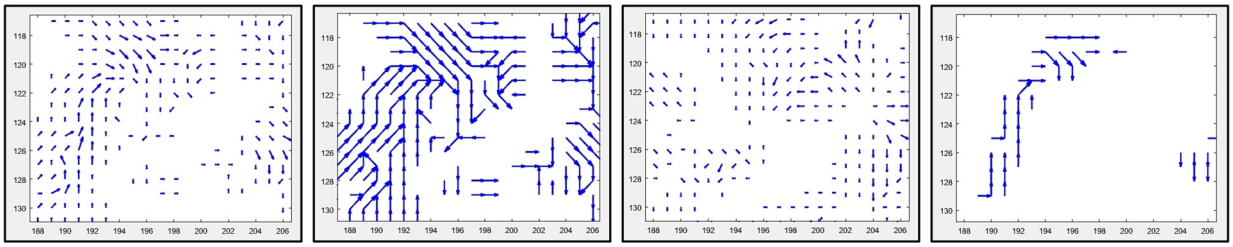


***Fig.10:*** *The zoomed-in dense optical flow vectors of the AKIYO image frame no. 50 which it is interfered by Speckle noise (variance 0.05) processed by (a) H-S, (b) M-HS, (c) B-HS, and (d) L-HS.*

the outcome for Speckle (variance 0.01 and 0.05) is shown. This sequence presents rapid movement and changing of the camera angle during the frame no. 67 to 88 that caused the high errors.

We experimented with the FOREMAN sequence in Fig. 5. Fig.5(a) illustrates the Poisson finding. In Fig.5(b) and Fig.5(c), the outcome for Salt-Pepper (density 0.005 and 0.025) is shown. In Fig.5(d) and Fig.5(e), the outcome for Speckle (variance 0.01 and 0.05) is shown.

We experimented with the AKIYO sequence in Fig.6. Fig.6(a) illustrates the Poisson finding. In Fig.6(b) and Fig.6(c), the outcome for Salt-Pepper (density 0.005 and 0.025) is shown. In Fig.6(d) and Fig.6(e), the outcome for Speckle (variance 0.01 and 0.05) is shown.

We experimented with the CONTAINER sequence in Fig.7. Fig.7(a) illustrates the Poisson finding. In Fig.7(b) and Fig.7(c), the outcome for Salt-Pepper (density 0.005 and 0.025) is shown. In Fig.7(d) and Fig.7(e), the outcome for Speckle (variance 0.01 and 0.05) is shown.

We segmented the measurement result into categories based on the different types of noise present in each set of the input video sequence. Additionally, we looked at and contrasted the EVM values for each robust approach, including H-S, M-HS, B-HS, and L-HS. Table 1 summarizes the outcome using the EVM's average and standard deviation. In Fig. 8, the average EVM data is represented the ploted graph for comparison.

Fig. 9 illustrates the optical flow vectors from each method (H-S, M-HS, B-HS, and L-HS) of AKIYO image frame no. 50 that was interfered by Spackle Noise (variance 0.05). And the zoomed-in dense optical flow is presents in Fig. 10.

## 4. CONCLUSION

H-S's motion flow is significantly impacted by non-Gaussian noises. The Salt-Pepper has the greatest influence on determining the motion flow using H-S. At the higher density of Salt-Pepper noise, the result of EVM keeps increasing. In comparison, the Poisson and the Speckle have a smaller impact. The robustness approaches offer extremely high benefits for finding the motion flow by H-S over non-Gaussian noises. Both the M-HS and the L-HS perform well in terms of robustness, and their robustness levels are comparable. The robustness levels of the M-HS and the L-HS appear to be equal when we consider certain noise types like Poisson. The M-HS appears to be more efficient for Salt-Pepper. However, when we examine the SD, the L-HS appears to have a more consistent result. By the way, with a steadier SD, the L-HS achieves the best resilience against Speckle noise.

We find that the characteristic of the video sequence also affected differently by different type of the non-Gaussian noise. In the slow movement sequences such as AKIYO and CONTAINER, they receive higher impact than the fast movement sequences such as COASTGUARD and FOREMAN.

When we consider the dense optical flow vectors, the robustness approaches present the removal of the

error vector cause by noise. With B-HS, it maintains the found vectors from H-S while M-HS and L-HS strengthen the vector. But the L-HS present better result for removing the vector error in the background image that was interfered by non-Gaussian noise.

We conclude that the L-HS is acknowledged as a different, reliable method for determining motion flow in non-Gaussian noises.

## ACKNOWLEDGEMENT

This research project was funded by Assumption University of Thailand (Tel: +66 2-300-4543).

## References

[1] A. Burton and J. Radford, "Thinking in Perspective: Critical Essays in the Study of Thought Processes," *Optical Flow*, Routledge, 1978.

[2] D.H. Warren and E. R. Strelow, "Electronic Spatial Sensing for the Blind: Contributions from Perception," *Optical Flow*, Springer, 1985.

[3] T.R. Reed *et.al.*, "Digital Image Sequence Processing, Compression, and Analysis," *Compression techniques*, Chemical Rubber Company (CRC) Press, 2005.

[4] B.D. Lucas and T. Kanade, "An Iterative Image Registration Technique with an Application to Stereo Vision," in *Proc. Defense Advanced Research Projects Agency (DARPA) Image Understanding Workshop*, pp. 121-130, 1981.

[5] D.J. Fleet and A.D. Jepson, "Computation of component image velocity from local phase information," *Computer Vision*, vol.5, pp.77-104, 1990.

[6] B.K.P. Horn and B.G. Schunck, "Determining Optical Flow," *Artificial Intelligence*, vol.17, pp.185-203, 1981.

[7] K. Blachut and T. Kryjak, "Real-Time Efficient FPGA Implementation of the Multi-Scale Lucas-Kanade and Horn-Schunck Optical Flow Algorithms for a 4K Video Stream," *Journal on the science and technology of sensors (Sensors)*, vol.13 no.13, July 2022.

[8] R.K. Bhogal and V. Devendran, "Real-Time Efficient FPGA Implementation of the Multi-Scale Lucas-Kanade and Horn-Schunck Optical Flow Algorithms for a 4K Video Stream," in *Proc. 2023 International Conference on Intelligent Data Communication Technologies and Internet of Things (IDCIoT)*, Jan. 2023.

[9] Z. Chen, T. He, X. Jin and F. Wu, "Learning for Video Compression," in *IEEE Transactions on Circuits and Systems for Video Technology*, vol. 30, no. 2, pp. 566-576, Feb. 2020.

[10] A.J. Qasim *et.al.*, "Review on techniques and file formats of image compression," *Bulletin of Electrical Engineering and Informatics*, vol. 9, no. 2, April 2020.

[11] Royden *et.al.*, "Use of speed cues in the detection of moving objects by moving observers," *Vision Research*, vol.59, 2012, pp. 17–24.

[12] P. Saeyong and K. Thongpull, "Visual SLAM Framework with Culling Strategy Enhancement for Dynamic Object Detection," *ECTI-CIT Transactions*, vol. 17, no. 3, September 2023, pp. 398–408.

[13] L. Lu and W. Zhou, "A Novel Efficient Mode Selection Approach for H.264," *Journal of Software Engineering and Applications*, vol.3, no.5, 2010.

[14] "Information Technology-Coding of Audio Visual Objects-Part 2: Visual," *MPEG-4 Visual.* ISO/IEC 14496-2:2004, 2004.

[15] P.S.M. Skelton *et.al.*, "Consistent estimation of rotational optical flow in real environments using a biologically-inspired vision algorithm on embedded hardware," *Image and Vision Computing*, vol.92, December 2019, 103814.

[16] D. Kesrarat *et.al.*, "A Novel Elementary Spatial Expanding Scheme Form on SISR Method with Modifying Geman&Mcclure Function," *TELKOMNIKA*, Indonesia, vol.17, no.5, Oct. 2019.

[17] V. Patanavijit and K. Thakulsukanant, "A Computational Experimental Investigation of Noise Suppressing Technique Stand on Hard Decision Threshold Dissimilarity under Fixed-Intensity Impulse Noise," *Indonesian Journal of Electrical Engineering and Computer Science (IJEECS), Institute of Advanced Engineering and Science (IAES)*, vol.23 (4), Oct. 2021.

[18] V. Patanavijit and K. Thakulsukanant, "The Novel Noise Classification Techniques Found on QTSD (Quadruple Threshold Statistical Detection) Filter under FIIN Environment," *Bulletin of Electrical Engineering and Informatics (BEEI), Institute of Advanced Engineering and Science (IAES)*, vol.10 (5), Oct. 2021.

[19] L. Abderrahim *et.al.*, "Novel design of a fractional wavelet and its application to image denoising," *Bulletin of Electrical Engineering and Informatics*, vol. 9, no. 1, Feb. 2020.

[20] T. Kondo and W. Kongpawechnon, "Robust Motion Estimation Methods Using Gradient Orientation Information," *ScienceAsia 35 (Journal of The Science Society of Thailand)*, pp. 196-202, 2009.

[21] D. Kesrarat and V. Patanavijit, "Noise resistance evaluation of spatial-field optical flow using modifying Lorentzian function," *Bulletin of Electrical Engineering and Informatics*, vol.11, no.5, pp. 2603-2610, Oct. 2022.

[22] S. Paris *et.al*, "Bilateral filtering: Theory and Applications," *Found. Trends Compt. Graph. Vis.*, vol. 4, no. 1, pp.1-73, , 2008.

[23] M. G. Mozerov, "Constrained Optical Flow Estimation as a Matching Problem," in *IEEE Transactions on Image Processing*, vol. 22, no. 5, pp. 2044-2055, May 2013.

[24] J. Sun, et.al., "Symmetric stereo matching for occlusion handling," in *Proc. IEEE Conf. Comput. Vis.Pattern Recognit.*, pp. 399-406, 2005.

[25] J. Sun, Y. Li, S. B. Kang and H.-Y. Shum, "Symmetric stereo matching for occlusion handling," *2005 IEEE Computer Society Conference on Computer Vision and Pattern Recognition (CVPR'05)*, San Diego, CA, USA, pp. 399-406, vol. 2, 2005.

[26] D. Kesrarat and V. Patanavijit, "Experimental Analysis of Non-Gaussian Noise Resistance on Global Method Optical Flow using Bilateral in Reverse Confidential," *Bulletin of Electrical Engineering and Informatics*, vol. 10, no.2, pp.716-723, Apr. 2021.

[27] P. J. Huber, "Robust Statistics," New York: Wiley, 1981.

[28] M. J. Black, G. Sapiro, D. H. Marimont and D. Heeger, "Robust anisotropic diffusion," in *IEEE Transactions on Image Processing*, vol. 7, no. 3, pp. 421-432, Mar. 1998.

[29] A. N. A. Rahim *et.al.*, "Improving the iterative back projection estimation through Lorentzian sharp infinite symmetrical filter," *International Journal of Electrical and Computer Engineering*, vol. 12, no. 3, pp. 2539-2552, Jun. 2022,

[30] J. L. Barron, D. J. Fleet, and S. S. Beauchemin, "Performance of Optical Flow Techniques," *International Journal of Computer Vision*, vol. 12, pp. 43-77, 1994.

**Darun Kesrarat** received the B.S., M.S., and Ph.D. from the Department of Information Technology at Assumption University, Bangkok, Thailand. He is currently an Assistance Professor. His research areas include signal processing on image/video reconstruction, super-resolution reconstruction (SRR), motion estimation, and optical flow estimation. He can be contacted at email: darunksr@gmail.com

**Vorapoj Patanavijit** received the B.Eng., M.Eng. and Ph.D. degrees from the Department of Electrical Engineering at the Chulalongkorn University, Bangkok, Thailand, in 1994, 1997 and 2007 respectively. He has served as a full-time lecturer at Department of Electrical and Electronic Engineering, Faculty of Engineering, Assumption University since 1998 where he is currently an Associate Professor. He works in the field of signal processing and multidimensional signal processing, specializing, in particular, on Image/Video Reconstruction, SRR (Super-Resolution Reconstruction), Compressive Sensing, Enhancement, Fusion, Digital Filtering, Denoising, Inverse Problems, Motion Estimation, Optical Flow Estimation and Registration. He can be contacted at email: patanavijit@yahoo.com

**Kornkamol Thakulsukanant** received the B.Eng. (Electrical Engineering) from Assumption University, Thailand in 1994, MSc.(Telecommunications and Computer Network Engineering) from London South Bank University, United Kingdom in 1997 and Ph.D. (in Electronic and Electrical Engineering) from Bristol University, United Kingdom in 2009 respectively. She works in the field of Digital Signal Processing (DSP) and Digital Image Processing (DIP), specializing, in particular, on Digital Image Reconstruction/Enhancement. She can be contacted at email: kthakulsukanant@yahoo.com